Noname manuscript No.
(will be inserted by the editor)

Upward propagation of very lean methane-air flames in vertical tubes

V. Muntean · F. J. Higuera

Received: date / Accepted: date

Abstract The upward propagation of a lean methane-air flame front in a vertical tube is investigated. The velocity of the flame front has been measured with an array of photodiodes set along the tube wall and, independently, from photographic records. A PIV system triggered by a photodiode signal has been used to measure the velocity of the flow induced by the flame front in a vertical plane through the axis of the tube. The contour of the luminous region of the flame front, assumed cylindrically symmetric, has been extracted from the recorded images. As expected, the shape and velocity of a very lean flame front, and the velocity of the fresh gas relative to the front, are similar to those of a bubble rising in the tube. The flow of the burnt gas features a region of low velocity (relative to the flame front) which enhances radiation losses and seems to play an important role in the extinction of the flame at the flammability limit. This limit is found to depend very sensitively on the temperature of the tube wall. A simple model is proposed of the flow around the axis of the tube and the combustion around the tip of the flame front. This model uses the measured gas velocity at the axis of the tube together with simplified conservation equations to compute the temperature and species concentrations along the axis for a given kinetic scheme and radiation law. The results for a single overall Arrhenius reaction and for a four-step reduced scheme, both in an optically thin gas, are in reasonable agreement with our experimental data and shed some light on the roles played by radiation losses and kinetic effects on the flammability limit measured in the standard flammability tube. The model can also be used to test other kinetic schemes and radiation laws.

Keywords Lean premixed flames · Upward propagation · Flammability limit.

1 Introduction

The upward propagation of a premixed flame front in a long vertical tube which is open at the bottom, closed at the top, and filled with a very lean reactive mixture

E. T. S. Ingenieros Aeronáuticos, UPM, Plaza Cardenal Cisneros 3, 28040 Madrid, Spain
E-mail: fhiguera@aero.upm.es

is a much studied problem. It arises in connection with the standard flammability tube first proposed by Coward and Jones [1] as a means to characterize the flammability of gas mixtures. Buoyancy plays a dominant role in the motion of these flame fronts. Levy [2] noted that for most fuels, hydrogen excepted, the shape and velocity of near-limit flame fronts are similar to those of a bubble rising in a tube filled with a liquid, as determined by Davies and Taylor [3]. Extinction at the flammability limit begins at the tip of the flame front, and the flammability limit depends on the radius of the tube. Thus, in their experiments with ammonia-air and propane-air mixtures, Babkin et al. [4] found that the minimum possible concentration of the reactant that is depleted by the flame increases with the radius of the tube for lean ammonia-air mixtures and rich propane-air mixtures, while it decreases with the radius of the tube for rich ammonia-air mixtures and is nearly independent of the radius for lean propane-air mixtures. Attempts at explaining extinction in terms of flame stretch date back to Lewis and von Elbe [5], while von Lavante and Strehlow [6] numerically found that the stretch is dominated by the strain rate of the flow and is of the right order to affect the inner structure of the flame (see Ref. [7] for a more recent computation). However, the strain rate of the buoyancy-dominated flow scales with the inverse of the square root of the tube radius (see, e.g. Ref. [8]), which suggests that, in some cases, when the Lewis number of the reactant that is depleted by the flame is above unity, the concentration of this reactant at the flammability limit should increase when the radius of the tube decreases (see, e.g. Buckmaster and Mikolaitis [8] and Williams [9]). This is contrary to some of the results of Refs. [1] and [4], among others. The issue was taken up by Shoshin et al. [10], who explained observed trends by the fact that the coupled effect of positive flame stretch and preferential diffusion locally strengthens the tip of the flame in mixtures with Lewis number (of the deficient reactant) below unity, and weakens it in mixtures with Lewis number above unity. These authors concluded that flame stretch and preferential diffusion alone cannot always account for the observed fact that extinction of a limit flame begins at its tip. Later, Shoshin and Jarosinski [11] and Shoshin et al. [12] proposed that heat losses from the flame due to the effect of radiation in a low velocity region that appears below very lean flames may explain the observed extinction.

In this paper, we report an experimental investigation of very lean methane-air flame fronts propagating upward in a tube. The velocity of the flame front and the velocity field of the flow it induces in the tube are measured using photographic and PIV techniques. A simple model of the flow around the tip of the flame front is proposed that uses the measured velocity of the gas together with approximate energy and species conservation equations to compute the temperature and species concentration profiles along the axis of the tube. Assuming a four-step reduced scheme, an optically thin gas, and transparent tube walls, this model gives predictions for the flammability limit that are in good agreement with our experiments, and partially supports the view that radiation losses are responsible for extinction in the standard flammability tube. The model can also be used as a workbench to test more realistic chemical kinetics and heat losses.

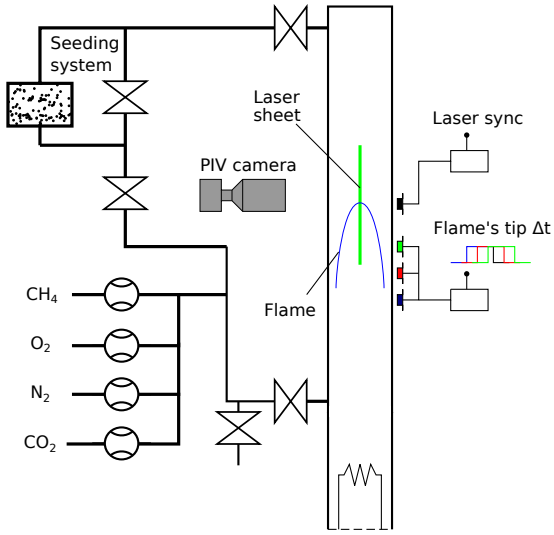

Fig. 1 Sketch of the experiment

2 Methods

2.1 Experimental setup and techniques

Figure 1 is a sketch of our experimental setup. The central element is a vertical quartz tube of 54 mm internal diameter, 3 mm wall thickness, and 1.9 m long, whose lower end is open to the atmosphere. In each run, the tube is filled through a valve at its top with a mixture of methane and air of chosen equivalence ratio, which is prepared from 99.5-pure methane, oxygen and nitrogen, whose flow rates are measured separately using EL-Flow Bronkhorst mass flow controllers. The accuracy of these controllers is 0.5% of the reading plus 0.1% of the apparatus' span. However, the flow rates of oxygen and nitrogen are set to the constant values 2.52 l_n/min and 9.48 l_n/min, respectively, the same in all the experimental runs, which are independently measured with an accuracy of 0.5% by means of Ritter TG10 Drum-type gas meters used to calibrate the oxygen and nitrogen Bronkhorst controllers at flow rates near those used in our experiments. (Here l_n denotes liters referenced to normal conditions; a temperature of 0 °C and a pressure of 101325 Pa). The flow rate of methane changes from run to run, as this is the means used to change the equivalence ratio of the mixture. However, these changes are small, the methane flow rate being in the range from 0.7 l_n/min to 0.8 l_n/min, which is about a 2% of the capacity of the methane controller. The mid value of this range is independently measured with an accuracy of 0.2% by means of the Ritter TG05 gas meter used to calibrate the methane controller. Thus it is expected that the combination of calibration and a reduced apparatus span will decrease the error of the methane flow rate measurements to about 2% × 0.6% = 0.012% of the full span. The typical error of the equivalence ratio is then 1%. Error bars of this variable are included in Fig. 2 below.

The fresh mixture flows through the top of the tube with a velocity of about 0.1 m/s for at least three minutes, to evacuate the burnt gas from previous runs. The volume of mixture used amounts to 10 times the volume of the tube, and no difference was observed if the fresh gas is kept flowing longer or if this gas is left in the tube for some time after closing the valve. A CO_2 probe shows that the concentration of this species left in the tube from previous runs rapidly decreases when the fresh mixture begins to flow.

After the valve at the top is closed, the lower 15 cm of the tube are filled with an enriched mixture through a second valve that opens at this height. The purpose of the enriched mixture is to facilitate ignition and to smooth the transition of the flame to the region of the tube filled with the mixture of interest. The device has been used by others before (e.g., Levy [2], Shoshin et al. [10], Shoshin and Goey [13]). When the filling process is complete, the mixture in the tube is allowed to settle for about two minutes and is ignited with an electrical resistance near the lower end of the tube. Transition from the enriched mixture to the test mixture of interest occurs in a region that may extend somewhat above the lower valve, due to the turbulence and diffusion that act following the filling of the lower part of the tube. As in Ref. [13], where the use of an enriched mixture to launch the flame is discussed in some detail, the length of this transition region is judged by the distance between the lower valve and the location at which the flame approaches quasi-steady shape and speed. As in Ref. [2], the flame was observed to fail at most a few tube diameters above the lower valve when the upper part of the tube is filled with a non-flammable mixture. These tests suggest that inhomogeneity of the gas mixture due to the enriched mixture present at the lower part of the tube does not extend to the test region where the measurements described below are made. The toroidal eddy found in Ref. [10] for a 24 mm tube, which rises with the flame and carries gas from the lower to the upper part of the tube, was not observed in our experiments, but see further comments on this point in section 3.

The upward velocity of the flame front (but not its shape) was measured by two means. On the one hand, an array of photodiodes was set along the tube which are sequentially excited by the passage of the flame, despite its weak luminosity. On the other hand, the motion of the flame front was recorded by a video camera that images a region of the tube about 40 cm long. The flame velocities measured by the two methods are in good agreement and show that the flame rises steadily after an initial transient.

The shape of the flame front (assumed cylindrically symmetric) was determined from the images of a second camera fitted with a large aperture objective (Tamron, 60 mm) that images a shorter region of the tube of about 68 mm with a resolution of 40–70 pixel/mm and is triggered once per run by the signal of a photodiode that detects the passage of the flame at a lower section of the tube. Tests have shown that an exposure time of 1.5 ms with a f-number of 2.0 allows to gather enough light from the faint flame to clearly detect its contour without causing blur. The upward velocity of the flame front is about 23 cm/s (see Fig. 2 below) and the thickness of the unstretched flame is about 1.5 mm. The Canny algorithm [14] with a Laplacian of Gaussian filter was used to extract the contour of the flame front from the recorded images.

A PIV system was used to measure the velocity of the gas around the flame front in a vertical plane through the axis of the tube. The PIV camera (nac Memrecam HX-3) images the same region of the tube as the camera used to determine

the contour of the flame with a resolution of 32 pixel/mm. The two cameras and the pulsed Nd:YAG laser of the PIV system were triggered by the same photodiode signal. The gas mixture was seeded with alumina particles, which were produced in a fluidized bed inserted in the gas line some distance upstream of the valve at the top of the tube. The density of seeding was tuned to optimize the quality of the PIV correlations by changing the fraction of gas that bypasses the fluidized bed. This optimization was not always possible because the thermal expansion of the gas across the flame drastically changes the seeding density, and sometimes makes it necessary to use different seedings to determine the velocities upstream and downstream of the flame in different runs.

Seeding the gas with solid particles may have an influence on radiation losses, which could significantly affect the experiment as radiation losses from the combustion products already seem to play an important role in the extinction of the flame at the flammability limit. The properties, conditions and number density of the seeding particles are not accurately known, which makes it difficult to directly evaluate radiation losses from these particles. However, flame front speeds measured for nominally identical cases with and without particles, and the flammability limit determined with and without particles, coincide within the experimental uncertainty, which suggests that radiation from the seeding particles has no significant effect on the flame at the density of seeding used.

Thermophoretic forces on the seeding particles are a cause of systematic error in LDV and PIV measurements in regions with strong temperature gradients (Talbot et al. [15], Beresnev and Chernyak [16]). Pending a comprehensive assessment of the effect of thermophoresis in our experiment, preliminary tests with various particle sizes suggest that thermophoresis does not drastically affect the measured gas velocity within the flame when the seeding particles are larger that a few microns.

The temperatures of the tube and the gas were measured at different sections of the tube with type-T (Cu–CuNi) thermocouples. These measurements have been used to study the nonuniform cooling of the tube following the passage of a flame, and to determine the minimum time required between runs. It was found that temperature variations of a few degrees may have an effect on the propagation of near limit flames.

2.2 Approximate model

A simple model is set up to approximately describe the flow and the near limit flame in a region around the axis of the tube, where extinction first occurs at the flammability limit. The model relies on a combination of experimental results and simplified conservation equations. It gives reasonable results and serves as a workbench where different kinetic and heat losses models can be compared and tested.

Previous work (Peters and Rogg [17]) has shown that a four step reduced chemical kinetics mechanism with three intermediate species out of steady state suffices to describe most aspects of lean premixed flames. Here, following Sánchez et al. [18], we choose OH as the radical representative of the H_2–O_2 radicals pool and take CO, H_2 and OH as the three intermediate species out of steady state.

This yields the four-step reduced scheme

$$\mathrm{CH_4 + 2\,OH \rightarrow CO + H_2O + 2\,H_2} \tag{1}$$
$$\mathrm{H_2 + O_2 \leftrightharpoons 2\,OH} \tag{2}$$
$$\mathrm{2\,OH + H_2 \leftrightharpoons 2\,H_2O} \tag{3}$$
$$\mathrm{CO + H_2O \leftrightharpoons CO_2 + H_2} \tag{4}$$

with rates (moles per unit volume per unit time)

$$\omega_1 = (k_{1_1}\,[\mathrm{H}] + k_{1_2}\,[\mathrm{OH}])\,[\mathrm{CH_4}] \tag{5}$$
$$\omega_2 = k_{2f}\,[\mathrm{O_2}]\,[\mathrm{H}] - k_{2b}\,[\mathrm{O}]\,[\mathrm{OH}] \tag{6}$$
$$\omega_3 = (k_{3f}\,[\mathrm{O_2}]\,[\mathrm{H}] - k_{3b}\,[\mathrm{HO_2}])\,[\mathrm{M}] \tag{7}$$
$$\omega_4 = k_{4f}\,[\mathrm{CO}]\,[\mathrm{OH}] - k_{4b}\,[\mathrm{CO_2}]\,[\mathrm{H}] \tag{8}$$

where $[i]$ denotes the molar concentration of species i, $[\mathrm{M}] = 0.6[\mathrm{H_2}] + 0.4[\mathrm{N_2}] + 0.44[\mathrm{H_2O}] + 0.4[\mathrm{O_2}] + 1.5[\mathrm{CO_2}] + 3[\mathrm{CH_4}] + [\mathrm{OTHERS}]$ is the effective third body concentration, and the molar concentrations of H, O and $\mathrm{HO_2}$ that appear in (5)–(8) are given by

$$\left.\begin{aligned} [\mathrm{H}] = K_1\frac{[\mathrm{H_2}]\,[\mathrm{OH}]}{[\mathrm{H_2O}]}, \qquad [\mathrm{O}] = K_2\frac{[\mathrm{OH}]^2}{[\mathrm{H_2O}]}, \\ [\mathrm{HO_2}] = \frac{k_{3f}\,[\mathrm{M}]\,[\mathrm{H}] + k_{5b}\,[\mathrm{H_2O}]}{k_{3b}\,[\mathrm{M}] + k_{5f}\,[\mathrm{OH}]}\,[\mathrm{O_2}]\,, \end{aligned}\right\} \tag{9}$$

which are simplified forms of more complex relations derived from the conditions of partial equilibrium and steady state of some reactions and species (see Ref. [18] for details). The reaction constants coincide, with minor changes, with those used in Ref. [18] to compute the structure and speed of planar flames at high temperature and pressure.

Consider the stationary flow of the gas at the axis of the tube in a reference frame moving with the flame front. Approximate energy and species conservation equations along the axis read

$$\left.\begin{aligned} \rho v c_p\frac{\mathrm{d}T}{\mathrm{d}x} = \frac{\mathrm{d}}{\mathrm{d}x}\left(\lambda\frac{\mathrm{d}T}{\mathrm{d}x}\right) + \alpha\lambda\frac{T_b - T}{R^2} + W_{_T} - L, \\ \rho v\frac{\mathrm{d}Y_i}{\mathrm{d}x} = \frac{\mathrm{d}}{\mathrm{d}x}\left(\frac{\lambda/c_p}{\mathrm{Le}_i}\frac{\mathrm{d}Y_i}{\mathrm{d}x}\right) + W_i, \end{aligned}\right\} \tag{10}$$

where x is downward vertical distance; $v(x)$ is the downward velocity of the gas relative to the flame; ρ and T are the gas density and temperature; $Y_i = \mathcal{M}_i[i]/\rho$ and Le_i are the mass fractions and Lewis numbers of the seven species $i = \mathrm{O_2, CH_4, CO_2, H_2O, CO, H_2}$ and OH, with $\mathcal{M}_i$ denoting the molecular masses of these species; c_p and λ are the specific heat and thermal conductivity of the gas; and the reaction and radiation terms $W_{_T}$, L and W_i on the right-hand sides of the equations will be discussed below. The following approximations have been made to write these equations: (*i*) Radial diffusion of species and heat are neglected in the transport region of the flame, which seems reasonable when the thickness of this region is small compared to the curvature radius of the flame front; (*ii*) radial diffusion of species is neglected downstream of the flame, where the gradients of

the species concentrations are small; (*iii*) radial heat conduction is approximated by $\alpha\lambda\,(T_b - T)\,/R^2$ downstream of the flame, where T_b is the final combustion temperature, R is the radius of the tube, and $\alpha = 15$ ($\alpha = 0$ upstream of the flame). This α is a model parameter, and its value is chosen for the results to fit a limited number of axisymmetric simulations carried out with the full mass, momentum and energy conservation equations. Equations (10) are to be solved together with the equation of state

$$\sum_i \frac{Y_i}{\mathcal{M}_i}\,\rho T = \sum_i \frac{Y_{i_u}}{\mathcal{M}_i}\,\rho_u T_u \tag{11}$$

and the boundary conditions (in terms of the equivalence ratio ϕ)

$$\left.\begin{aligned} T - T_u = Y_{CO_2} = Y_{H_2O} = Y_{CO} = Y_{H_2} = Y_{OH} = 0 \\ Y_{CH_4} = Y_{CH_4 u} = \frac{\phi}{17.167 + \phi} \\ Y_{O_2} = Y_{O_2 u} = \frac{4}{17.167 + \phi} \end{aligned}\right\} \tag{12}$$

for $x \to -\infty$, with the subscript u denoting conditions of the fresh gas far above the flame front, and

$$\frac{\mathrm{d}T}{\mathrm{d}x} = \frac{\mathrm{d}Y_i}{\mathrm{d}x} = 0. \tag{13}$$

for $x \to \infty$.

The production rates on the right-hand sides of (10) are $W_{_T} = q_1\omega_1 + q_2\omega_2 + q_3\omega_3 + q_4\omega_4$, with $q_1 = 356.082$ kJ/mole, $q_2 = -78.852$ kJ/mole, $q_3 = 562.043$ kJ/mole, and $q_4 = 41.114$ kJ/mole, $W_{_{O2}} = -\mathcal{M}_{_{O_2}}\,\omega_2$, $W_{_{CH_4}} = -\mathcal{M}_{_{CH_4}}\,\omega_1$, $W_{_{CO_2}} = \mathcal{M}_{_{CO_2}}\,\omega_4$, $W_{_{H_2O}} = \mathcal{M}_{_{H_2O}}(\omega_1 - \omega_4)$, $W_{_{CO}} = \mathcal{M}_{_{CO}}(\omega_1 - \omega_4)$, $W_{_{H_2}} = \mathcal{M}_{_{H_2}}(2\,\omega_1 - \omega_2 - \omega_3 + \omega_4)$, and $W_{_{OH}} = \mathcal{M}_{_{OH}}(-\omega_1 + \omega_2 - \omega_3)$. Since nitrogen is by far the most abundant species, only binary diffusion of each species in nitrogen is considered, with constant Lewis numbers $\mathrm{Le}_{_{O_2}} = 1.05$, $\mathrm{Le}_{_{CH_4}} = 1$, $\mathrm{Le}_{_{CO_2}} = 1.39$, $\mathrm{Le}_{_{H_2O}} = 0.83$, $\mathrm{Le}_{_{CO}} = 1.07$, $\mathrm{Le}_{_{H_2}} = 0.3$, $\mathrm{Le}_{_{OH}} = 0.74$, and a thermal conductivity $\lambda = \lambda_u\,(T/T_u)^{\kappa}$ with $\kappa = 0.75$ and $\lambda_u = 2.53 \times 10^{-2}$ N s^{-1} K^{-1}.

The last term on the right-hand side of the energy equation in (10) represents the radiation losses,

$$\left.\begin{aligned} L = 4\sigma K\left(T^4 - T_u^4\right) \quad \text{with} \\ K = \rho R^0 T\left(K_{_{CO_2}}\frac{Y_{_{CO_2}}}{\mathcal{M}_{_{CO_2}}} + K_{_{H_2O}}\frac{Y_{_{H_2O}}}{\mathcal{M}_{_{H_2O}}}\right), \end{aligned}\right\} \tag{14}$$

where an optically thin gas and transparent tube wall are assumed. Here σ and R^0 are the Stefan-Boltzmann constant and the universal gas constant, and the Planck mean absorption coefficient K is taken from Ju et al. [19], who evaluated it with the statistical narrow band model (Fiveland [20], Soufiani and Taine [21]). We assume, in addition, that radiation is due only to the reaction products CO_2 and H_2O. The factors $TK_{_{CO_2}}$ and $TK_{_{H_2O}}$ depend only weakly on temperature.

Computations carried out with the four step reduced kinetics for planar flames without radiation losses ($1/R = L = 0$, ρv uniform) show that the solution of (1)–(13) almost exactly reproduces the flame speed of the GRI-Mech 3.0 scheme

implemented in the Cantera software (see www.cantera.org) for values of the equivalence ratio below 0.7, and gives profiles of temperature and the seven species whose evolution is computed that are in good agreement with those derived from the complete kinetic scheme.

A simpler kinetic scheme has been also used consisting of a single overall Arrhenius reaction that gives $W_T/q = W_{CO_2}/(11/4) = W_{H_2O}/(9/4) = -W_{CH_4} = \rho Y_{CH_4} B \exp(-T_a/T)$, with activation temperature $T_a = 18750$ K (in line with Ref. [22]), frequency factor B chosen to have a planar flame velocity $U_L = 4.63$ cm/s for $T_u = 300$ K and $Y_{CH_4 u} = 0.03$ (see, e.g. Ref. [23]), and $q = 5.01 \times 10^4$ kJ/kg.

A momentum equation would be needed to close the problem and compute the velocity $v(x)$, which in turn would require information on the pressure at the axis of the tube. Here this equation is replaced by the experimentally measured velocity profile.

For the numerical treatment, Eqs. (10) are discretized using finite differences on a uniform grid of 1000 points in the axial range of Fig. 3(b) below, which gives a grid spacing of 0.05 mm. The position of the flame relative to the velocity profile is given by choosing the point, say x_0, where the scaled temperature $\theta = (T - T_u)/\Delta T$, with $c_p \Delta T = (q_1 + 2q_2 + q_3 + q_4) Y_{CH_4 u}/\mathcal{M}_{CH_4}$, takes a certain value, typically 0.8, and the equivalence ratio in (12) is iteratively computed to satisfy this condition. The point x_0 is then changed and the computation is repeated until the mass flux ρv varies smoothly across the flame. The value of ϕ thus determined is compared to the known equivalence ratio for the experimental run from which the velocity profile was extracted. The difference is a measure of the accuracy of the method and the simplified kinetic and heat losses in (1)–(8) and (14).

3 Results and discussion

The recorded shape of the flame front consists of a rounded cap similar to a bubble rising in the tube followed by a long skirt; a shape often reported in the literature. Inspection of a number of flames shows that, in most cases when ignition is produced symmetrically and care is taken to minimize residual motions of the gas in the tube and thermal perturbations through the tube wall, the flame front tends to rise steadily and to take a nearly axisymmetric form after an initial transient. Asymmetries in the flame skirt near the wall could not be avoided.

The velocity of the flame front, U_0, is shown in Fig. 2 as a function of the equivalence ratio, ϕ. Values of the velocity obtained from the photographic records and from the array of photodiodes coincide within the experimental error. The data in Fig. 2 are averages over at least five runs for each value of the equivalence ratio. Also shown in this figure is the ratio of the average length of the skirt, H, measured on the recorded images, to the radius of the tube, R.

For the lean mixtures considered here, the velocity U_0 is nearly independent of the equivalence ratio and close to the velocity of a bubble rising steadily in the tube. For a tube of 54 mm and a heavy-to-light fluid density ratio of 5, which is about the burnt-to-fresh gas temperature ratio for ϕ in the range of Fig. 2, this velocity is $U_{DT} = 22$ cm/s, from Davies and Taylor formula [3]. The velocity of the flame relative to the fresh gas, u_f say, should be of the order of the unstretched flame velocity in the fresh mixture. This is small compared to U_0, of the order of a

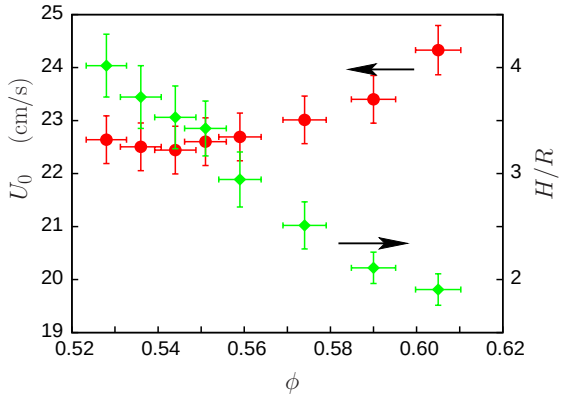

Fig. 2 Upward velocity of the flame front, U_0 (red), and ratio of the length of the flame to the radius of the tube, H/R (green, right-hand side scale), as functions of the equivalence ratio of the mixture, ϕ. The values shown are averages over several flames for each equivalence ratio. The error bars show the dispersion of the results, which increases when ϕ decreases. The minimum ϕ in the figure is slightly above the flammability limit that we find when the tube is allowed to cool down between runs.

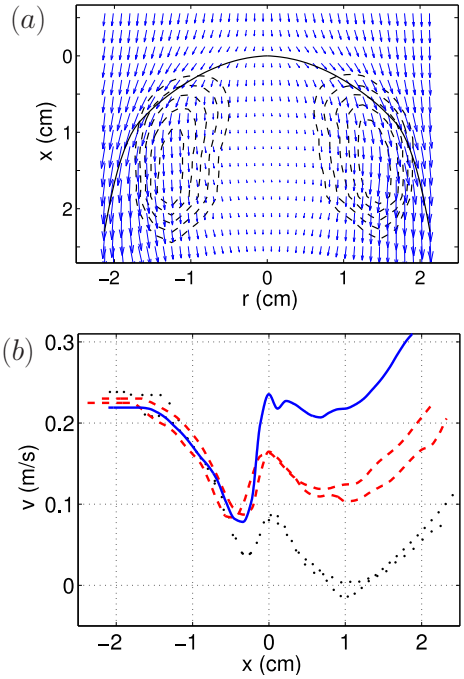

Fig. 3 (*a*) Velocity of the gas relative to the flame (arrows), contours of constant vorticity (dashed), and contour of the luminous region of the flame (solid), for $\phi = 0.53$. (*b*) Velocity relative to the flame front along the axis of the tube for $\phi = 0.55$ (solid), 0.54 (dashed), and 0.53 (dotted). Different profiles, corresponding to different runs, are shown for each value of ϕ to give an idea of the error of the measurements. The origin of vertical distance is set at the local velocity maximum.

few centimeters per second, though it increases rapidly with ϕ. As a consequence, the tip of the flame front is confined to a neighborhood of the stagnation point of the equivalent bubble flow, and the rest of the flame front lies near the streamline across this point. The decrease of H/R with increasing ϕ is in qualitative agreement with the estimate $H/R \sim U_0/u_f$ derived from mass conservation.

The small increase of U_0 for the two leftmost points of Fig. 2 may be an effect of the ignition conditions which is brought to bear by the small velocity of the burnt gas relative to the near limit flame (see below). Because of this small velocity, some of the gas from the bottom of the tube may accompany the flame during a significant part of its evolution and, since this gas carries part of the excess of energy used for ignition, it mildly aids flame propagation. The effect is inherent to the structure of the flow behind a near limit flame. It may partially account for the sensitivity of the flammability limit to experimental conditions [1].

Figure 3(a) shows a sample velocity field of the gas relative to the flame front. This velocity is obtained subtracting the velocity of the front U_0 from the velocity of the gas relative to the tube, measured with PIV. The dashed curves in Fig. 3(a) are vorticity contours. Also included in this figure is the contour of the luminous region of the flame (solid curve), which has been extracted from the images of the flame and fitted using least squares splines.

The downward velocity of the gas relative to the flame at the axis of the tube is shown in Fig. 3(b) for three values of the equivalence ratio. Different profiles for the same value of the equivalence ratio correspond to different experimental runs and give an idea of the magnitude of the experimental error. As can be seen, the velocity of the gas first decreases on approaching the flame front from above, as it would do for a rising bubble; then increases on crossing the flame front, due to the gas thermal expansion; decreases again downstream of the flame, due to the buoyancy force acting on the burnt gas; and finally increases at some distance downstream of the flame front, due to the convergence of the burnt gas that crossed the flame at different points of the front (see velocity arrows in Fig. 3(a)).

The velocity of the gas ahead of the flame front changes little when the concentration of methane is changed. However, the velocity of the burnt gas undergoes more important changes. A region of low velocity is apparent in Fig. 3(a) downstream of the flame, and the size of this region increases when the methane concentration decreases. Recirculation in the reference frame tied to the flame front was seldom observed in these experiments, though it has been often observed in experiments with narrower tubes [10]. In any case, the existence of a low velocity region reflects a competition between buoyancy, which pushes the hot gas upward around the axis of the tube, and the downward flow that emerges from the flame front with a velocity of order $u_b = \rho_u u_f/\rho_b$ (from mass conservation across the flame, with ρ_u and ρ_b denoting the densities of the fresh and burnt gases). The latter flow has no analogue for a rising bubble. The pressure variations arising in this flow are of order $\Delta p_b = \rho_b u_b^2$, while the pressure variations in the fresh gas above the flame front are of order $\Delta p_u = \rho_u U_0^2$. Both u_f/U_0 and the ratio $\Delta p_b/\Delta p_u = O\left[(\rho_u/\rho_b)(u_f/U_0)^2\right]$ are small for very lean flames, which explains the similarity of the fresh gas flow and the shape of the flame with those of a bubble. Buoyancy dominates the upward motion of the flame front and the flow of the fresh gas.

The residence time of the hot gas in the low velocity region may be very large. This increases radiation losses, which cool down the slowly moving gas and may

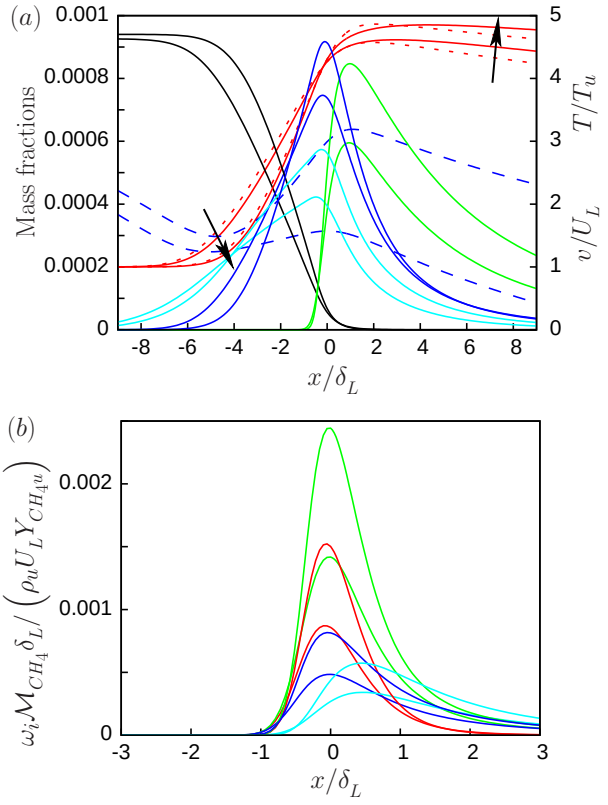

Fig. 4 (a): Profiles of temperature (red, right-hand scale) and mass fractions of CH_4 (divided by 30, black), CO (divided by 15, dark blue), OH (green), and H_2 (multiplied by 10, light blue) computed as functions of downward distance using the velocity profiles (dashed blue, right-hand scale) measured for $\phi \approx 0.53$ and 0.54, increasing from bottom to top or as indicated by the arrows. (b): Rates of steps 1 (red), 2 (green), 3 (dark blue), and 4 (light blue) of the four step reduced scheme. The values of the equivalence ratio determined from the semianalytical model are $\phi_{model} = 0.509$ and 0.519, respectively. Dotted red curves in (a) are the temperature profiles computed with the single step kinetics. Temperatures are scaled with $T_u = 300$ K, velocities with the reference flame velocity $U_L = 4.63$ cm/s, distance with the reference flame thickness $\delta_L = \alpha_u / U_L = 4.32 \times 10^{-2}$ cm, with $\alpha_u = 0.2$ cm^2/s, and reaction rates with $\rho_u (Y_{CH_4 u} / \mathcal{M}_{CH_4}) U_L / \delta_L$. The origin of x is at the point where θ defined in section 2.2 equals 0.8.

have an influence on the flame, even if the concentrations of radiating species (mainly CO_2 and H_2O) are very small; see below.

Figure 4(a) shows temperature (red) and species concentration profiles computed with the simplified model (1)–(14), together with the measured velocity profiles used in these computations (dashed blue). Results are shown for two values of the equivalence ratio, $\phi \approx 0.53$ and 0.54, the lower one being close to the minimum for which a flame front can propagate in the tube for a wall temperature of 26^o C. The values of the equivalence ratio determined by the model are $\phi_{model} = 0.509$ and 0.519, respectively, which are somewhat smaller than the real values and give an idea of the error of the model. For the same values of the equiv-

alence ratio, Fig. 4(b) shows the rates (5)–(8) of the four-step reduced scheme as functions of the distance along the axis of the tube. Step 2 (green) represents radicals production through the hydrogen-oxygen chain, while step 3 (dark blue) represents radicals recombination. Radicals are also consumed to attack the fuel (step 1, red). The sum of the rates of steps 1 and 3 nearly coincides with the rate of step 2, implying that OH is not far from steady state. The rates of all three steps decrease when the flame temperature is decreased by decreasing the equivalence ratio, but the rate of step 2, which has a large activation energy, decreases the most and the rate of the three-body step 3 decreases the least. Effective combustion ceases to be possible when radicals removal stops the fuel attack step 1, which happens below a certain cross-over temperature; see Refs. [17,18]. The results in Fig. 4(b) show that this condition is approached when ϕ is decreased, but the rate of step 1 remains larger than that of step 3 at the smallest values of ϕ attained. Moreover, additional computations carried out for the same velocity profiles with the single reaction scheme, for which no cross-over temperature exists, give temperature profiles (dotted red curves in Fig. 4(a)) very similar to those of the four step scheme, which casts some doubts on the kinetic extinction account.

Due to radiation losses, the maximum computed temperature is lower than the adiabatic temperature of the planar flame (T_{eq}, with $T_{eq}/T_u = 5.12$ and 5.19 for the two cases shown in Fig. 4) by an amount of the order of the Frank-Kamenetskii temperature, T_{eq}^2/T_a, which is $0.42\,T_u$ for the lower value of ϕ and the activation temperature of the single reaction scheme. Thus the flame is clearly nearing extinction (see, e.g. Williams [9]), but the weak dependence of the temperature profile on the kinetic scheme suggests that shortage of radicals needs not be the factor that unleash extinction; it may rather occur when the fate of the flame is already decided.

The strong effect of the radiation may be surprising at first sight. Acting on a planar flame, the radiation losses considered here would decrease the final combustion temperature by an amount $\delta T = O\left[\lambda_b L_b/(\rho_u c_p u_f)^2\right]$, where L_b is the radiation loss (14) evaluated in the burnt gas (at $T = T_b$, $Y_{H_2O} = 9\,Y_{CH_4u}/4$, $Y_{CO_2} = 11\,Y_{CH_4u}/4$) and u_f is the flame velocity; see Williams [9]. With u_f of the order of the adiabatic flame velocity and $T_b \approx T_{eq}$, this gives $\delta T/(T_b - T_u) = O(2.5 \times 10^{-2})$, which is too small to extinguish the flame. The enhanced effect of radiation losses for near limit flames is connected to the low velocity region that appears downstream of these flames, as first noted by Shoshin and Jarosinski [11] and Shoshin et al. [12]. Inspection of the convection, conduction and radiation terms of the energy equation (10) downstream of the flame [24] shows that a convection-radiation balance analogous to that of a planar flame is approached for values of ϕ well above the flammability limit, but this balance changes to a conduction-radiation balance near the flammability limit because convection becomes small in the low velocity region. In these conditions, the decrease of the final combustion temperature is given by the modified estimate

$$\delta T = O\left(\frac{L_b \ell}{\rho_u c_p u_f}\right), \tag{15}$$

where ℓ is the characteristic size of the low velocity region, of the order of the radius of the tube. This modified estimate follows from an enthalpy balance across the flame, $\rho_u u_f c_p \delta T = q_b$, where q_b is the heat conduction flux from the flame to the burnt gas, which is of order $L_b \ell$ when conduction and radiation matter in

the low velocity region. This δT is larger than the estimate quoted above for a planar flame by a factor ℓ/δ_b, where $\delta_b = \lambda_b/\rho_u c_p u_f$ is the flame thickness. This factor can easily be of the order of 20 or higher, which makes δT larger than the Frank-Kamenetskii temperature and accounts for the results in Fig. 4.

Table 1 Mass fraction of methane and equivalence ratio at the flammability limit for various values of the N_2:O_2 volume ratio.

N_2:O_2	0	0.9	1.0	2.9	3.8	5.3	6.2
$Y_{CH_4 u}$	0.031	0.030	0.030	0.030	0.030	0.031	0.031
ϕ	0.13	0.14	0.23	0.44	0.54	0.72	0.82

Additional experiments have been done to further assess the effect of radiation losses. Experiments with various values of the fresh gas N_2:O_2 volume ratio show that the mass fraction $Y_{CH_4 u}$ is nearly constant at the flammability limit, while the equivalence ratio increases with the nitrogen dilution; see Table 1. This result can be accounted for noticing that (*a*) a global enthalpy balance shows that the temperature difference $T_{eq} - T_u$ is proportional to $Y_{CH_4 u}$ and independent of the N_2:O_2 ratio if small changes of the specific heat and very small concentrations of unreacted species in the equilibrium mixture are left out; and (*b*) the radiation losses (14) are proportional to the mass fractions of the radiating species, whose values in the hot burnt gas are in turn proportional to $Y_{CH_4 u}$. Thus, if radiation losses are relevant, the difference $T_b - T_u$, where $T_b = T_{eq} - \delta T$ is the final combustion temperature, and the whole structure of the flow, should depend only on $Y_{CH_4 u}$ and not on the dilution. In particular, $Y_{CH_4 u}$ should have a constant value at the flammability limit, in agreement with the experimental results. The final combustion temperature T_b is also predicted to be constant at the flammability limit, but we cannot measure this quantity in our experiments.

Table 2 Mass fraction of methane at the flammability limit for various values of the mass fraction of CO_2 in the fresh gas. In all the cases $([N_2] + [CO_2])/[O_2] = 3.76$ in the fresh gas.

$Y_{CO_2 u}$	0.057	0.072	0.092	0.11	0.14
$Y_{CH_4 u}$	0.03	0.031	0.032	0.032	0.033

Experiments have also been carried out replacing part of the N_2 of the fresh gas with CO_2, liter per liter. Table 2 shows that the mass fraction of methane at the flammability limit increases with the concentration of CO_2 in the fresh gas. A line of slope $s = \mathrm{d}Y_{CH_4 u}/\mathrm{d}Y_{CO_2 u} \approx 0.035$ can be fitted to the data. These results reflect the competition of two opposing factors. On the one hand, radiation losses are increased by adding CO_2, both directly, due to the presence of this species already in the fresh gas, and indirectly, due to the additional radiating species produced by the combustion of the additional CH_4. On the other hand, the additional CH_4 strengthens the flame. The rates of decrease of the final combustion temperature due to enhanced losses and of increase due to the increased methane concentration can be estimated and compared.

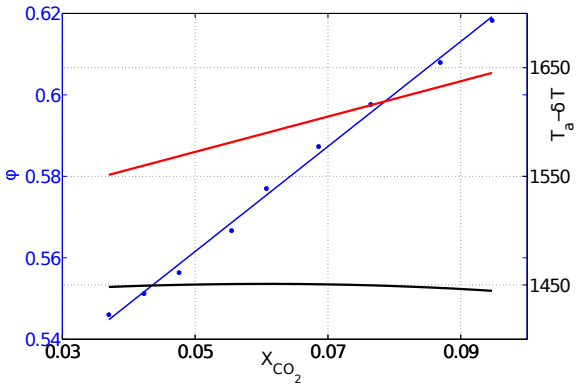

Fig. 5 Measured equivalence ratio (blue, left-hand scale) and estimated flame temperature at the flammability limit (black, right-hand scale) as functions of the mole fraction of CO_2 added to the fresh gas. The red curve gives the adiabatic flame temperature.

- The sensitivity of the radiation losses in (14) to the added CO_2 can be approximated by $L_b' = \left(\partial L_b/\partial Y_{CO_2}\right)[1 + (44/16)s] + \left(\partial L_b/\partial Y_{H_2O}\right)(2\times 18/16)s$, where the factors proportional to s account for the additional mass of CO_2 and H_2O present in the burnt gas due to the combustion of the additional CH_4. Carrying this approximation to the estimate (15) of the decrease of the final combustion temperature due to radiation losses, we find $\delta T' = \mathrm{d}\left(\delta T\right)/\mathrm{d}Y_{CO_2u} = O\left(L_b'\ell/\rho_u c_p u_f\right)$.
- The rate of variation of the adiabatic flame temperature due to the variation of Y_{CH_4u} that accompanies the variation of Y_{CO_2u} for the limit flame is $T_{eq}' = \mathrm{d}T_{eq}/\mathrm{d}Y_{CO_2u} \approx sq/c_p$.

Using the experimental value of s and replacing ℓ and u_f in the estimate of $\delta T'$ with the radius of the tube and the adiabatic flame velocity computed with the Cantera software, the ratio $\delta T'/T_{eq}'$ comes out of order unity for near limit flames. This shows the important role played by radiation losses. When the losses are increased by increasing Y_{CO_2u}, the strength of the flame must be increased by increasing Y_{CH_4u} in order to offset these losses.

Figure 5 shows the values at the flammability limit of the equivalence ratio (blue curve), the adiabatic flame temperature (T_{eq}, red curve), and an estimated final combustion temperature (black curve). This temperature is obtained by subtracting from T_{eq} the value δT estimated in (15) [with $L(T_{eq})$ evaluated from (14) at the equilibrium composition of the mixture] multiplied by an arbitrary factor. The estimated final combustion temperature is nearly independent of the concentration of CO_2 for a certain value of this factor.

4 Conclusions

The upward propagation of a lean methane-air flame front in a vertical tube has been investigated using photographic records and PIV to measure the shape and velocity of the flame front and the velocity of the gas around the front.

A simple semianalytical model of the temperature and species mass fractions along the axis of the tube has been proposed which uses the measured velocity of the gas. This model gives reasonable predictions of the flammability limit, in agreement with our experimental data, and suggests that extinction at the flammability limit may be fairly independent of kinetic details.

Series of experiments have been carried out in which the N_2:O_2 volume ratio of the fresh gas is varied or part of the N_2 is replaced by CO_2. The mass fraction of methane at the flammability limit is found to be nearly independent of the N_2:O_2 ratio and to increase with the concentration of CO_2 in the fresh gas, which supports the view that radiation losses are important at the flammability limit measured with the standard flammability tube.

Acknowledgements This work was supported by the Spanish MINECO through projects CSD2010-00010 and DPI2013-47372-C02-02.

References

1. H. F. Coward and G. H. Jones, *Limits of flammability of gases and vapors,* U. S. Bureau of Mines Bull. #503, 1952.
2. A. Levy, An optical study of flammability limits, *Proc. R. Soc. London A* 283, 134–145, 1965.
3. R. M. Davies and G. I. Taylor, The mechanics of large bubbles rising through extended liquids and through liquids in tubes, *Proc. R. Soc. London A* 200, 375–390, 1950.
4. V. S. Babkin, V. V. Zamashchikov, A. M. Badalyan, V. N. Krivulin, E. A. Kudryavtsev and A. N. Baraton, Effect of tube diameter on homogeneous gas flame propagation limits, *Combustion, Explosions and Shocks Waves* 18, 164–171, 1982.
5. B. Lewis and G. von Elbe, *Combustion, Flames and Explosions of Gases,* Academic Press, New York, 1961, Chap. 5.
6. E. von Lavante and R. A. Strehlow, The mechanism of lean limit flame extinction, *Combust. Flame* 49, 123–140, 1983.
7. F. J. Higuera, Numerical simulation of the upward propagation of a flame in a vertical tube filled with a very lean mixture, *Combust. Flame* 158, 885–892, 2011.
8. J. Buckmaster and D. Mikolaitis, A flammability-limit model for upward propagation through lean methane/air mixtures in a standard flammability tube, *Combust. Flame* 45, 109–119, 1982.
9. F. A. Williams, *Combustion Theory*, 2nd ed. Benjamin Cummings, Menlo Park, CA, 1985.
10. Y. L. Shoshin, L. Tecce and J. Jarosinski, Experimental and computational study of lean limit methane-air flame propagating upward in a 24 mm diameter tube, *Combust. Sci. Technol.* 180, 1812–1828, 2008.
11. Y. L. Shoshin and J. Jarosinski, On extinction mechanism of lean limit methane-air flame in a standard flammability tube, *Proc. Combust. Inst.* 32, 1043–1050, 2009.
12. Y. L. Shoshin, G. Gorecki, J. Jarosinski and T. Fodemski, Experimental study of limit lean methane/air flame in a standard flammability tube using particle image velocimetry method, *Combust. Flame* 157, 884–892, 2010.
13. Y. L. Shoshin and L. P. H. de Goey, Experimental study of lean flammability limits of methane/hydrogen/air mixtures in tubes of different diameters, *Exp. Thermal Fluid Sci.* 34, 373–380, 2010.
14. J. Canny, A computational approach to edge detection, *IEEE Trans. Pattern Analysis Machine Intelligence* PAMI-8, 679–698, 1986.
15. L. Talbot, R. K. Cheng, R. W. Schefer and D. R. Willis, Thermophoresis on particles in a heated boundary layer, *J. Fluid Mech.* 101, 737–758, 1980.
16. S. Beresnev and V. Chernyak, Thermophoresis of a spherical particle in a rarefied gas: Numerical analysis based on the model kinetic equations, *Phys. Fluids* 7, 1743–1756, 1985.
17. N. Peters and B. Rogg, Reduced Kinetic Mechanisms for Applications in Combustion Systems, Lecture Notes in Physics m15, Springer Verlag, Berlin. 1993.

18. A. L. Sánchez, A. Lépinette, M. Bollig, A. Liñán and B. Lázaro, The reduced kinetic description of lean premixed flames. *Combust. Flame* 123, 436–464, 2000.
19. Y. Ju, H. Guo, F. Liu and K. Maruta, Effects of the Lewis number and radiation heat loss on the bifurcation and extinction of CH_4/O_2–N_2–He flames, *J. Fluid Mech.* 379, 165–190, 1999.
20. W. A. Fiveland, Discrete-ordinates solutions of the radiative transport equation for rectangular enclosures, *ASME J. Heat Transfer* 106, 699–706, 1984.
21. A. Soufiani and J. Taine, High temperature gas radiative property parameters of statistical narrow-band model for H_2O, CO_2 and CO, and correlated K-model for H_2O and CO_2. *Int. J. Heat Mass Transfer* 40, 987–991, 1997.
22. C. K. Westbrook and F. L. Dryer, Simplified reaction mechanisms for the oxidation of hydrocarbon fuels in flames, *Combust. Sci. Technol.* 27, 31–43, 1981.
23. S. G. Davis, J. Quinard and G. Searby, Markstein numbers in counterflow, methane- and propane-air flames: a computational study, *Combust. Flame* 130, 123–136, 2002.
24. F. J. Higuera and V. Muntean, Effect of radiation losses on very lean methane/air flames propagating upward in a vertical tube, *Combust. Flame* 161, 2340–2347, 2014.